energies

MDPI

Article

Health-Conscious Optimization of Long-Term Operation for Hybrid PEMFC Ship Propulsion Systems

Chiara Dall'Armi, Davide Pivetta and Rodolfo Taccani *

Department of Engineering and Architecture, University of Trieste, via Valerio 10, 34127 Trieste, Italy; chiara.dall'armi@phd.units.it (C.D.); davide.pivetta@phd.units.it (D.P.)
* Correspondence: taccani@units.it

Abstract: The need to decarbonize the shipping sector is leading to a growing interest in fuel cell-based propulsion systems. While Polymer Electrolyte Membrane Fuel Cells (PEMFC) represent one of the most promising and mature technologies for onboard implementation, they are still prone to remarkable degradation. The same problem is also affecting Lithium-ion batteries (LIB), which are usually coupled with PEMFC in hybrid powertrains. By including the combined degradation effects in an optimization strategy, the best compromise between costs and PEMFC/LIB lifetime could be determined. However, this is still a challenging yet crucial aspect, rarely addressed in the literature and rarely yet explored. To fill this gap, a health-conscious optimization is here proposed for the long-term minimization of costs and PEMFC/LIB degradation. Results show that a holistic multi-objective optimization allows a 185% increase of PEMFC/LIB lifetime with respect to a fuel-consumption-minimization-only approach. With the progressive ageing of PEMFC/LIB, the hybrid propulsion system modifies the energy management strategy to limit the increase of the daily operation cost. Comparing the optimization results at the beginning and the end of the plant lifetime, daily operation costs are increased by 73% and hydrogen consumption by 29%. The proposed methodology is believed to be a useful tool, able to give insights into the effective costs involved in the long-term operation of this new type of propulsion system.

Keywords: PEMFC degradation; lithium-ion battery degradation; health-conscious optimization; hybrid PEMFC ship propulsion; MILP approach; RO-Pax ferry

Citation: Dall'Armi, C.; Pivetta, D.; Taccani, R. Health-Conscious Optimization of Long-Term Operation for Hybrid PEMFC Ship Propulsion Systems. *Energies* **2021**, *14*, 3813. https://doi.org/10.3390/en14133813

Academic Editors: Viktor Hacker and Tomaž Katrašnik

Received: 27 May 2021
Accepted: 23 June 2021
Published: 24 June 2021

1. Introduction

In the last few decades, an increasing number of restrictions has been introduced in the transportation sector in order to reduce greenhouse gases and pollutant emissions. This has posed new technological challenges, and the need to explore new solutions is ever more urgent. In particular, growing efforts have been placed in reducing the emissions of the shipping sector, where the new and upcoming restrictions require a thorough revision of the whole ship building process. The urge to develop and upscale new technological solutions for decarbonizing the maritime transportation sector has promoted the research and development of different strategies. Among them, fuel cell-based propulsion has gained attention, as was demonstrated by several national and international initiatives on this topic [1–4]. As emerged from a previous study by the authors [3], one of the most promising solutions employs hydrogen-fuelled Polymer Electrolyte Membrane Fuel Cells (PEMFC), hybridized with a Battery Energy Storage System (BESS). In fact, it is well known that hydrogen-fueled PEMFC can potentially guarantee zero-emission propulsion: this feature makes their use fully compliant even to the most stringent regulations. As has already been demonstrated in several analyses, a small to medium sized vessel could benefit from the installation of hybrid PEMFC/BESS propulsion systems. In fact, the technical and regulatory barriers are currently limiting the installed power of PEMFC to few hundred kW, as highlighted in Table 1 and extracted from [3]. As for BESS, Table 1

also points out that the most recent projects use Lithium-Ion Batteries (LIB), as LIB are the commercial product with the best characteristics in terms of specific energy [5].

Table 1. List of projects on hybrid PEMFC/BESS propulsion systems. Elaborated from [3].

Project Name	Start Date	End Date	PEMFC Power	Battery Type and Capacity	Ref.
Elektra and Elektra 2 (e4ships consortium)	2017	2024	300 kW	LIB, 2.5 kWh capacity	[6,7]
Energy observer	2017	2024	22 kW	LIB, 122 kWh propulsion, 18 kWh daily facilities	[8,9]
Aero 42	-	2023	2800 kW	LIB, 672 kWh	[10,11]
Race for water	2015	2021	60 kW	LIB, 745 kWh	[12]
Future Proof Shipping	-	2021	635 kW	LIB, 300 kWh	[13]
Kamine boat	2018	2020	60 kW	LIB, 60 kWh	[14,15]
Water Go Round Golden Gate Zero Emission	-	2020	360 kW	100 kWh, no data on the type	[16,17]
Zeff (part of Pilot-E scheme)	2018	2020	2200 kW	50 kWh estimated; type of batteries under evaluation	[18,19]
Zero V	-	2017	1800 kW	LIB provide for 200 kW power	[20,21]
Busan tourist boat	-	2016	56 kW	LIB, 47 kWh	[22]
ZEMSHIP FSC Alsterwasser	2006	2013	100 kW	Lead gel, 560 V (7 × 80 V) 360 Ah	[23–25]
Nemo H2	2008	2011	60–70 kW	Lead acid, 55 kW	[26]

The main drawback of such hybrid PEMFC/LIB powertrains is that both PEMFC and BESS are prone to degradation, which is responsible for the overall reduction of the plant lifespan. Hence, a correct design and management of hybrid PEMFC/LIB powertrains is fundamental in order to achieve their cost effectiveness [27,28]. The management of hybrid PEMFC/LIB powertrains also includes the energy-efficient power allocation, usually addressed by the definition of an Energy Management Strategy (EMS). The latter can be defined following different approaches, among which rule-based and optimization-based ones are the most investigated in the literature on ship propulsion systems.

As for rule-based EMSs, an example is provided by Taccani et al. [29], who analyzed the implementation of a hybrid PEMFC/LIB power system for the propulsion of a small-sized ferry. The authors proposed a rule-based EMS in which PEMFC work at a constant load in order to cover the average power demand of the vessel, while LIB are used for peak shaving. Moreover, Han et al. [30] proposed a state-based EMS to control the energy flows between the PEMFC and the batteries of the hybrid ship Alsterwasser depending on the vessel power demand and the battery State of Charge (SOC) [23–25]. The same vessel was also studied by Bassam et al. [31], who proposed an improved state-based EMS for the hybrid PEMFC/battery system taking into account the PEMFC efficiency as input to the proportional-integral EMS. By adopting the proposed EMS, up to 3.5% of hydrogen daily consumption could be saved in comparison with a previously proposed strategy [30]. The main advantages of rule-based EMSs lie in their simplicity of use, which makes them practical for onboard applications. As a drawback, their operative principle is based on human expertise, and they could easily reflect human errors generated while defining the control strategy.

To overcome this issue, some studies proposed optimization-based EMSs [32–39]. For example, Rivarolo et al. [32,33] developed two computational tools dedicated to the

preliminary design and the thermo-economic analysis of different engineering solutions for ship power systems, including PEMFC and Solid Oxide Fuel Cells (SOFC). The proposed methodology provided the best energy system configuration in terms of environmental impact, cost, and overall dimensions. Bassam et al. [34] defined a multi-scheme EMS that minimizes the equivalent fuel consumption over one operation day of the hybrid PEMFC/BESS passenger ship Alsterwasser [23–25]. The developed EMS resulted in a 16.7% reduction of the total hydrogen consumption with respect to previously proposed EMSs. Zhang et al. [35] designed a real-time optimization EMS that took into account the degradation of PEMFC and used a high-pass filter to prolong battery life. A similar approach was followed by Chen et al. [36], who employed a whale optimization algorithm to optimize size and frequency for a hybrid battery/supercapacitor fuel cell ferry. Wu et al. [37] included the calculation of PEMFC degradation in the optimization of a hybrid plug-in PEMFC/BESS ferry for coastal navigation, defining the optimal size of the system by considering both greenhouse gas emissions and economic performances. For the same ferry, Wu et al. [38] recently proposed a reinforcement learning approach for the definition of an adaptive EMS. In both [37,38], the BESS degradation rate was set as a constant in each time step, independently from the operating conditions. Pivetta et al. [39] proposed a multi-objective design and operation optimization of three different ferries for coastal navigation, adopting a Mixed-Integer Linear Programming (MILP) approach based on a simultaneous minimization of PEMFC degradation, investment cost and operation cost. In this case, battery degradation was set as a constraint of the optimization model. As a main outcome, it was found that in order to limit both battery and PEMFC degradation, the battery capacity should be increased by up to 136%.

Although EMSs taking into account system degradation (also known as health-conscious EMSs) are of great interest for the shipping sector, the interplay between PEMFC and BESS degradation has been rarely addressed as of yet. Interesting contributions on this point can be found in the recent literature on hybrid PEMFC/BESS powertrains for other types of applications [40–47]. Some remarkable examples have been provided by Çinar et al. [43], Liang et al. [44], and Wang et al. [45]. The former group [43] used meta-heuristic algorithms to optimize hydrogen consumption in the aircraft sector. The second one [44] compared two EMSs (composite fuzzy control versus Pontryagin's minimum principle) for hybrid PEMFC/LIB logistics, while the third one [45] proposed a health-conscious EMS for a hybrid PEMFC/LIB bus. Both PEMFC and LIB degradation were included as the objectives in a cost-optimization problem. In addition, Li et al. [46] studied an online adaptive EMS for a PEMFC hybrid vehicle, which takes into account the degradation of PEMFC, batteries, and supercapacitors. The authors concluded that the degradation of one of the power sources implied an increase in the degradation of the other ones. Moreover, they proved that the proposed EMS guaranteed normal plant operation also in case of plant source degradation. However, a holistic analysis throughout the whole plant lifetime was not addressed, and a quantitative plant lifetime estimation was not provided. Lastly, a comprehensive review on health-conscious EMSs for hybrid fuel cell vehicles was proposed by Yue et al. [47], who concluded that future trends in this research field should address the multi-objective optimization of a hybrid PEMFC/LIB system including degradation modeling and lifetime estimation methods of the power sources, possibly limiting the overall complexity of the problem.

Overall, the literature review pointed out the importance of considering the degradation of both PEMFC and LIB in optimizing the entire hybrid ship-propulsion system. However, it emerged that a holistic optimization procedure that takes into account the progressive worsening of both PEMFC and BESS performances with the progressive ageing over the plant lifetime has not been addressed yet. This indeed would be fundamental for a complete understanding of the costs involved in the operation of hybrid PEMFC/LIB propulsion systems. To fill this gap, the present study proposes an innovative methodology that (i) evaluates the degradation over time of both PEMFC and LIB, (ii) optimizes the operation of a hybrid PEMFC/LIB powertrain over the entire lifetime, and (iii) simultaneously

minimizes the fuel consumption and the power source degradation rates. As is widely recognized, the MILP approach is a good candidate for optimizing complex energy systems because it allows a reduction in the computation effort with respect to other optimization techniques [48–51]. Therefore, in this study, MILP equations have been used to describe the hybrid PEMFC/LIB operation and a multi-objective optimization has been performed.

A small-size ferry for coastal navigation has been taken as case study to perform the optimization of operation over the entire power plant lifespan. The design of the system previously optimized in [39] has been taken as a reference for the operation optimization here proposed. Here, Lithium Iron Phosphate (LFP) chemistry has been chosen as LIB. Indeed, among different LIB chemistries Nickel Manganese Cobalt (NMC) and LFP batteries are addressed as the most mature technologies for shipping, but LFP are slightly better in terms of safety onboard [5].

The first part of the paper describes the methodology proposed for the analysis. Afterwards, the case study is described, and the results are presented and discussed.

2. Methodology

This section shows the main characteristics of the proposed method, with a particular focus on the equations describing the energy conversion and storage units. Given the complexity of the multi-objective optimization, a MILP approach has been adopted to limit the overall computational effort. Therefore, operation and performance degradation of the energy units, i.e., LFP battery and PEMFC, have been described with MILP equations. In the next paragraphs, a description of the procedure followed in the analysis is reported.

At first, the preliminary sizing of the hybrid PEMFC/LFP battery propulsion system has been determined by implementing the design and operation optimization model developed in [39]. The obtained sizes for PEMFC and LFP battery systems have been taken as input parameters of the new optimization approach for the long-term operation.

Starting from time $t_i = 0$, corresponding to a novel installation of both PEMFC and LFP battery, consecutive optimizations have been run in a loop until either PEMFC or LFP battery reached the end of their life. In order to limit the computational effort, it has been assumed that the first day of the month i is representative for the operation of all the days of the month (assuming all months have 30 days). Operation optimization has been performed for the day representative of the entire month i. The cumulative degradation of PEMFC and LIB calculated at the end of month i has been taken as an input parameter for the operation optimization of month $i + 1$.

The optimization problem has been developed in Python [52] and solved with the MILP optimizer Gurobi Optimization [53]. The general formulation of the MILP optimization problem has been set to find the optimal value of the generic continuous variables $\mathbf{x}^*(t)$ and binary variables $\boldsymbol{\delta}^*(t)$ that maximize or minimize the set objective function(s) Z (Equation (1)). The MILP problem is subject to equality constraints $\mathbf{g}(t)$ and inequality constraints $\mathbf{h}(t)$ (Equations (2) and (3)), which include the description of the modeled ship energy system. The continuous and binary variables represent the decision variables of the optimization problem. In particular, binary variables have been implemented to decide about activation/de-activation of each energy unit during operation.

$$Z = f(\mathbf{x}^*(t),\ \boldsymbol{\delta}^*(t)) \tag{1}$$

$$\mathbf{g}(\mathbf{x}^*(t),\ \boldsymbol{\delta}^*(t)) = 0 \tag{2}$$

$$\mathbf{h}(\mathbf{x}^*(t),\ \boldsymbol{\delta}^*(t)) \leq 0 \tag{3}$$

In the following subsections, the main constraints describing the energy system operation and the degradation models of PEMFC and LFP battery are presented, i.e., the relationships $\mathbf{g}(t)$ and $\mathbf{h}(t)$ in Equations (2) and (3). Subsequently, the objective functions of the optimization problem, i.e., the objective functions Z in Equation (1), and the solving procedure are illustrated and discussed.

2.1. Energy System Constraints

It has been assumed that at each time step t the ship energy demand $P_{demand}(t)$ (propulsion and auxiliaries power demand) is fulfilled by the power output of the n fuel cell stacks $P_{FC_j}(t)$ and by the discharging power of battery $P^{+}_{batt}(t)$. $P^{-}_{batt}(t)$ indicates the charging power of battery, which is charged by fuel cells whenever $P_{FC_i}(t)$ is higher than $P_{demand}(t)$. The overall power balance has been set as (Equation (4)):

$$\sum_{j=1}^{n} P_{FC_j}(t) + P^{+}_{batt}(t) = P_{demand}(t) + P^{-}_{batt}(t) \tag{4}$$

Equations (5) and (6) are the constraints adopted to limit the proposed energy system volume and weight, set to be lower than the values of volume V_{max} and weight w_{max} of the ferry existing energy system (i.e., internal combustion engines powered by marine gasoil). A correction factor (c_{ov}) has been introduced to consider the current limited development state of PEMFC and LFP battery technologies.

$$\sum_{j=1}^{n} \int_{t_{in}}^{t_{fin}} \left(F_{FC_j}(t) \cdot dt\right) \cdot V_{H_2} + E_{battery_{max}} \cdot V_{batt} + n \cdot P_{FC_{max}} \cdot V_{FC} \leq V_{max} \cdot (1 + c_{ov}) \tag{5}$$

$$\sum_{j=1}^{n} \int_{t_{in}}^{t_{fin}} \left(F_{FC_j}(t) \cdot dt\right) \cdot w_{H_2} + E_{battery_{max}} \cdot w_{batt} + n \cdot P_{FC_{max}} \cdot w_{FC} \leq w_{max} \cdot (1 + c_{ov}) \tag{6}$$

where t_{in} and t_{fin} identify the time interval considered for the operation of ferry without refueling. With reference to Equation (5), the volume occupied by hydrogen is expressed by $\int_{t_{in}}^{t_{fin}} (F_{FC_i}(t) \cdot dt) \cdot V_{H_2}$, where $F_{FC_j}(t)$ is the fuel consumption of the stack j at time t and V_{H_2} is the volume occupied by hydrogen and its storage system. The volume occupied by LIB is expressed as $E_{battery_{max}} \cdot V_{batt}$, where $E_{battery_{max}}$ is the energy capacity of the battery and V_{batt} is the specific volume. The volume required by PEMFC is determined as $n \cdot P_{FC_{max}} \cdot V_{FC}$, with n being the number of installed PEMFC stacks, $P_{FC_{max}}$ the fuel cell stack rated power and V_{FC} the specific volume of a PEMFC stack. Similarly, in Equation (6) the weight of hydrogen is expressed as $\int_{t_{in}}^{t_{fin}} \left(F_{FC_j}(t) \cdot dt\right) \cdot w_{H_2}$, being w_{H_2} the weight of bunkered hydrogen and its storage system. Weight of LIB is calculated as $E_{battery_{max}} \cdot w_{batt}$, where w_{batt} is the specific weight of LIB, and weight of PEMFC is $n \cdot P_{FC_{max}} \cdot w_{FC}$, where w_{FC} is the specific weight of PEMFC stack.

2.2. Polymer Electrolyte Membrane Fuel Cells Model

It has been considered that separate PEMFC stacks with fixed rated power are installed on board. Each stack has been assumed to operate independently from the others. Stacks with different rated power or with different performances could be included in the model by modifying the stack operation parameters (see Section 3).

The operation of the PEMFC stack j is described by the following MILP equations (Equations (7)–(11)):

$$F_{FC_j}(t) = \left(k_{1_F} \cdot I_{FC_j}(t) + k_{2_F}\right) \cdot \delta_{FC_j}(t) + \delta_{st,up_j}(t) \cdot F_{start} \cdot P_{FC_{max}} \tag{7}$$

$$P_{FC_j} = \left(k_{1_P} \cdot I_{FC_j}(t) + k_{2_P}\right) \cdot \delta_{FC_j}(t) \tag{8}$$

$$I_{FC_{min}} \cdot \delta_{FCj}(t) \leq I_{FC_j}(t) \leq I_{FC_{max}} \cdot \delta_{FC_j}(t) \tag{9}$$

$$\left|P_{FC_j}(t) - P_{FC_j}(t-1)\right| \leq \Delta_{P_{FC}} \tag{10}$$

$$0 \leq \delta_{FC_j}(t) - \delta_{FC_j}(t+1) + \delta_{st,up_j}(t) \tag{11}$$

where I_{FC_j} is the current density (in A/cm^2), k_{1F}, k_{2F}, k_{1P} and k_{2P} are the linearization coefficients, δ_{FC_j} is the binary variable defining on/off status, δ_{st,up_j} is the binary variable defining the occurrence of a start-up phase (if $\delta_{st,up_j} = 1$, it will be counted as one start/stop cycle), F_{start} is the fuel consumption in the start-up phase, $I_{FC_{min}}$ and $I_{FC_{max}}$ are the limiting values for the current density, and $\Delta_{P_{FC}}$ is the allowed load variation.

The PEMFC stack degradation is a complex phenomenon that affects the performances of several stack components (e.g., electrodes, membranes, bipolar plats, gas diffusion layers). Degradation effects may be different from one cell to another, e.g., near the edges, cells are subject to a faster degradation [54]. Besides, at the component level, the degradation mechanisms are hard to estimate. As reported in [47], the ageing mechanisms in mobility application could be analyzed through three possible approaches: impedance estimation based on electrochemical impedance spectrometry, remaining useful life estimation, and a stack voltage degradation model. Even though the latter approach is less accurate with respect to other degradation models and strongly depends on experimental data, voltage degradation can be expressed by MILP equations, allowing a sensible reduction of the computational effort required by an optimization with respect to, for example, Mixed-Integer Quadratic Programming (MIQP).

Therefore, the stack voltage degradation model has been adopted in this study to describe the PEMFC ageing. PEMFC voltage loss has been considered to depend mainly on three operating conditions: the stack load variation, the start/stop cycle and the idling/high-current operation of the stack [55]. The voltage loss caused by the stack degradation has been expressed as the voltage reduction of a single cell at an equal current density output, as proposed in other studies available in the literature [37,56–58].

Performance degradation of the PEMFC stack j at time t is described by Equations (12)–(15).

$$dV_{load_j}(t+1) = \left| P_{FC_j}(t) - P_{FC_j}(t+1) \right| \cdot \Delta v_{load} \tag{12}$$

$$dV_{st,up_j}(t) = \delta_{st,up_j}(t) \cdot \Delta v_{st,up} \tag{13}$$

$$dV_{P_{FC_j}}(t) = k_{1_{dv}} \cdot I_{FC_j}(t) + k_{2_{dv}} \tag{14}$$

$$dV_j(t) = dV_{load_j}(t) + dV_{st,up_j}(t) + dV_{P_{FC_j}}(t) \tag{15}$$

where $dV_{load_j}(t)$ is the voltage reduction due to load variation, Δv_{load} and $\Delta v_{st,up}$ are the proportionality constants, $dV_{st,up,j}(t)$ is the voltage reduction due to start-up, $dV_{P_{FC,j}}(t)$ is the voltage reduction depending on the power load, $k_{1_{dV}}$ and $k_{2_{dV}}$ are the linearization coefficients, $dV_j(t)$ is the total loss of voltage at time t.

The cumulative voltage degradation evaluated for the single cell modifies the characteristic curves of the entire stack. In particular, the relation between the cumulative loss of voltage (Equation (16)) and power has been approximated by a linear curve, which relates voltage loss to the angular coefficient of the power curve (k_{1_P}), as described in Equation (17). The SOH for PEMFC stack (SOH_{PEMFC_j}) has been defined as in Equation (18).

$$dV_{TOT,j} = \int dV_j(t) \cdot dt \tag{16}$$

$$k_{1_P} = k_{1_{deg}} \cdot dV_{TOT,j} + k_{2_{deg}} \tag{17}$$

$$SOH_{PEMFC_j} = \frac{V_{ref,FC} - dV_{TOT,j}}{V_{ref,FC}} \tag{18}$$

where $dV_{TOT,j}$ is the cumulative loss of voltage, $k_{1_{deg}}$ and $k_{2_{deg}}$ are the linearization coefficients, $V_{ref,FC}$ is the reference maximum voltage for a novel single cell (voltage at the minimum current density $I_{FC_{min}}$).

It has been assumed that k_{1_F} and k_{2_F} are not affected by the stack degradation $dV_{TOT,j}$. Therefore, when the power loss caused by degradation increases, the efficiency of the stack

tends to decrease. The stack efficiency η_{FC} has not been included as a decisional variable in the optimization problem, but it has been evaluated as a result (Equation (19)).

$$\eta_{FC} = P_{FC_j} / F_{FC_j} \tag{19}$$

2.3. Lithium Iron Phosphate Battery Model

At each time step t, the energy stored in the battery $E_{batt}(t)$ has been defined according to the charging/discharging power of the battery $P^{\pm}_{batt}(t)$ and the relative efficiency η_{batt}, assumed constant and equal in the charging/discharging phase (Equation (20)). The SOC of the battery at time t has been calculated as the ratio between $E_{batt}(t)$ and the energy capacity of the battery $E_{battery_{max}}$ (Equation (21)). The battery C-rate has been determined as the ratio between the charging/discharging power of the battery and the battery capacity (Equation (22)), and the C-rate has been constrained in order not to exceed the maximum C-rate ($Crate_{max}$) achievable by the battery (Equation (23)). A constraint has been set on the SOC in the first-time step of the day t_0 to make it correspond to the SOC at the end of the day t_{fin} (Equation (24)).

$$E_{batt}(t) = E_{batt}(t-1) + \left(\eta_{batt} \cdot P^{-}_{batt}(t) - (1/\eta_{batt}) \cdot P^{+}_{batt}(t)\right) \cdot \Delta t \tag{20}$$

$$SOC(t) = \frac{E_{batt}(t)}{E_{battery_{max}}} \tag{21}$$

$$Crate^{\pm}(t) = \frac{P^{\pm}_{batt}(t)}{E_{battery_{max}}} \tag{22}$$

$$\left|Crate^{\pm}(t)\right| \leq Crate_{max} \tag{23}$$

$$SOC(t_0) = SOC\left(t_{fin}\right) \tag{24}$$

As for battery degradation, the most dominant ageing phenomenon of LIB is the formation of a Solid Electrolyte Interface (SEI) at the electrode/electrolyte interface. The thickness of SEI increases over time, leading to a progressive increase in the impedance of the battery and a consequent decrease in the battery capacity. Different degradation models are available in the literature, based either on electrochemical/equivalent circuit methods (e.g., SEI film thickness models and internal resistance models), or on empirical/semi-empirical methods (e.g., capacity fade models) [47,59]. In this study, it has been chosen to model the battery degradation over time with a capacity fade model. In fact, such an approach allows to limit the overall computational burden with respect to electrochemical models, allowing a comprehensive analysis of the entire system.

Commonly, battery ageing can be classified into two categories: calendar ageing and cycle ageing. Calendar ageing occurs when the battery is at rest condition, i.e., when no current is flowing through the battery. Calendar degradation rates depend on SOC and temperature. Cycle ageing occurs when the battery is charged or discharged, and depends on battery C-rate, SOC, temperature, number of performed equivalent cycles, and Depth of Discharge (DOD) [60,61].

In the proposed study, the hybrid propulsion system has been considered to power a small-size ferry for public transport, which operates 24 h, seven days a week. Therefore, it is reasonable to assume that only cycle ageing occurs on the battery. Nevertheless, to prevent an excessive calendar ageing of the battery in case of a prolonged stop of the vessel it has been decided to set a constraint on the SOC at the end of each day of operation (Equation (25)). The reference SOC_{cal} has been set equal to 60%, according to the data available in the literature [62].

$$SOC\left(t_{fin}\right) = SOC_{cal} \tag{25}$$

Cycle ageing has been evaluated following the experimental studies available in [61] for a single LFP cell. As done for PEMFC (see Section 2.2), in this case it has also been considered in terms of the degradation of a single cell, representative for the whole battery. At each time step t of an operative day, $T_{batt}(t)$ has been expressed as linear function of $Crate(t)$, through the linearization coefficients $a_{1T,x}$ and $a_{2T,x}$ that depend on the ambient temperature (Equations (26) and (27)). The capacity fade of battery $Q_{loss}(t)$ has been calculated as a linear function of battery temperature $T_{batt}(t)$ (Equation (28)).

$$T_{batt}(t) = a_{1T,x} \cdot Crate(t) + a_{2T,\,x} \tag{26}$$

$$a_{1T,x} = f(T_{amb,x}); \;\; a_{2T,x} = f(T_{amb,x}) \tag{27}$$

$$Q_{loss\,i}(t) = a_{1QT,i} \cdot T_{batt}(t) + a_{2QT,i} \tag{28}$$

The time dependency of $Q_{loss}(t)$ in the long-term operation has been taken into account by determining the linearization coefficients $a_{1QT,x}$ and $a_{2QT,x}$ in Equation (27) at each month of the plant lifetime. In particular, $a_{1QT,x}$ and $a_{2QT,x}$ at the month i have been evaluated as a function of the energy throughput Ah_i at month I, as expressed in Equation (29).

$$a_{1QT,i} = k_{11,Ah} \cdot Ah_i^2 + k_{21,Ah} \cdot Ah_i \; + k_{31,Ah} \tag{29}$$

$$a_{2QT,i} = k_{12,Ah} \cdot Ah_i^2 + k_{22,Ah} \cdot Ah_i \; + k_{32,Ah} \tag{30}$$

where $k_{11,Ah}$, $k_{21,Ah}$, $k_{31,Ah}$, $k_{12,Ah}$, $k_{22,Ah}$, and $k_{32,Ah}$. Note that Equations (29) and (30) have been evaluated at the beginning of the optimization and hence have not been formulated as MILP. Equation (31) expresses the energy throughput Ah_i at month i.

$$Ah_i = n_{days} \cdot N_{cycle\,i-1} \cdot DOD \cdot Ah_{cell} \tag{31}$$

where n_{days} is the number of days per month (assumed all equal to 30 days), $N_{cycle_{i-1}}$ is the number of equivalent cycles performed by the battery during one operation day, representative for the month $i-1$. N_{cycle} has been determined via a rainflow algorithm. Ah_{cell} indicates the capacity of the single battery cell. DOD effect on the capacity fade has not been directly taken into account in the evaluation of $Q_{loss}(t)$, since its effect on the capacity fade is negligible if compared to the cycling effect [61]. As for the SOC effect, a constraint has been set (Equation (32)) to limit the SOC-window of operation and hence further limit the degradation, as proposed for example in [63].

$$SOC_{min} \; \leq SOC(t) \leq SOC_{max} \tag{32}$$

At the end of each month i, the SOH of the battery ($SOH_{battery_i}$) has been determined, as in Equation (32).

$$SOH_{battery_i} = \frac{E_{battery,max} - Q_{loss_i}}{E_{battery,max}} \tag{33}$$

2.4. Objective Functions

A multi-objective optimization has been performed to determine the optimal long-term operation of the proposed FC/LFP battery hybrid system, taking into account the fuel consumption and the degradation of both PEMFC and LFP battery over their lifetime.

Three objective functions have been specified, namely fuel consumption (f_1 in Equation (34)), PEMFC performance degradation (f_2 in Equation (35)), and LFP battery performance degradation (f_3 in Equation (36)). For the multi-objective optimization, a "Blended Objectives" method has been adopted, considering a linear combination of the objective functions, each with a fixed weight [53]. In this case, a cost-related weight has been assumed for each objective function. The weight of f_1 (w_1 in Equation (38)) depends on the cost of hydrogen. Weights of f_2 and f_3 (w_2 and w_3 in Equations (39) and (40)) derive from the cost of components and their lifetime. The multi-objective optimization has been performed

by minimizing the linear combination of the three objective functions, defined as f_{MO} (Equation (37)).

A 1% deviation from the optimal value of the f_{MO} function has been allowed.

$$f_1 = \sum_{j=1}^{n} \int_0^{t_{fin}} F_{FC_j}(t)\, dt \tag{34}$$

$$f_2 = \sum_{j=1}^{n} \int_0^{t_{fin}} dV_j(t) dt \tag{35}$$

$$f_3 = \int_0^{t_{fin}} Q_{loss\ battery}(t) dt \tag{36}$$

$$f_{MO} = Minimize\ (w_1 \cdot f_1 + w_2 \cdot f_2 + w_3 \cdot f_3) \tag{37}$$

w_i parameters have been defined as in Equations (38)–(40).

$$w_1 = c_{H_2} \tag{38}$$

$$w_2 = c_{FC} \cdot \frac{P_{FC_{max}}}{V_o} \tag{39}$$

$$w_3 = c_{batt} \cdot \frac{E_{battery,max}}{Q_{loss_{max}}} \tag{40}$$

where c_{FC} is the cost of a PEMFC stack (€/kW), and V_o is the total voltage loss permitted for the single cell of the PEMFC stacks (set equal to 20% of $V_{ref,FC}$). Similarly, c_{batt} is the cost of LFP battery (€/kWh), and $Q_{loss_{max}}$ is the maximum capacity fade of the battery (set equal to 20%).

3. Case Study

A typical small size RO-Pax (Roll-on/roll-off Passengers) ferry operating in coastal areas has been chosen as a case study. Table 2 reports the main characteristics of the ferry. The proposed RO-Pax is similar to the represented ferry in Figure 1. Power system volume and weight in Table 2 have been elaborated from data available on diesel storage on board and diesel-electric generator for marine propulsion, scaled by the installed power of the ferry.

Table 2. The main characteristics of the RO-Pax ferry proposed as a case study. Power system volume and weight have been elaborated from data available on diesel storage on board and a diesel-electric generator for marine propulsion, scaled by the installed power of the ferry.

	Unit	Value
Vessel Type	-	RO-Pax ferry
Length Overall	m	42
Breadth Extreme	m	9
Gross Tonnage	t	280
Propulsion engines	kW	2×206
Auxiliary engines	kW	2×28
Power system volume	m^3	15.5
Power system weight	kg	7185

Figure 1. A typical RO-Pax small size ferry.

The ferry power demands (propulsion and auxiliaries demands) over a typical operation day have been evaluated in [39]. Ferry power demands rated per minute enter as input in the proposed long-term operation optimization. More details on power profile and the typical sailing cycle of the ferry chosen as a case study are reported in Appendix A.

A simplified schematic of the propulsion system for the proposed case study is presented in Figure 2. Resulting from the design optimization performed in [39], the proposed energy system is composed of two 100-kW PEMFC stacks fueled by hydrogen, an energy management system, and a 286-kWh LFP battery. Hydrogen has been assumed to be stored in liquid form in a cryogenic tank, with the aim of reducing the volume and weight for the storage system in comparison to other types of hydrogen storage systems (e.g., compressed hydrogen tanks). It has been assumed that the ferry has enough fuel for a daily operation.

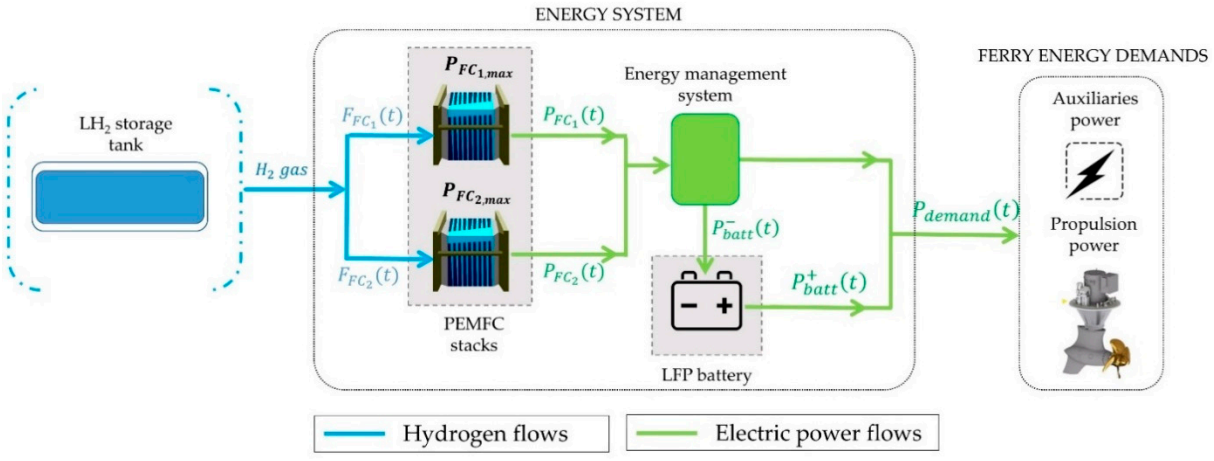

Figure 2. A simplified schematic of the proposed hybrid PEMFC/LFP battery propulsion system for the small-size ferry taken as a case study. Cryogenic tank provides hydrogen to two PEMFC stacks that convert chemical energy into electricity. The latter is sent to an energy management system that directs the power flows to fulfill the energy demand of the ferry (propulsion and auxiliaries demands) and/or to charge the battery.

The parameters that have been used for the long-term operation optimization are reported in Table 3. These model parameters represent the main characteristics of the considered ferry and of the current market scenario. In particular, the PEMFC and battery characteristics have been evaluated on the basis of the existing technologies.

Table 3. Input parameters of the multi-objective optimization.

Parameters	Unit	Value	Ref.
c_{H_2}	€/kWh	0.3	[64,65]
c_{batt}	€/kWh	818	[5,66]
c_{FC}	€/kW	3750	[64]
c_{ov}	%	20	Assumed
Δv_{load}	µV/kW	0.0441	[37,55–58]
$\Delta_{P_{FC}}$	%	10	Assumed
$\Delta v_{st,up}$	µV/cycle	23.91	[37,55–58]
Δt	min	1	Assumed
η_{batt}	%	90	Assumed
F_{start}	%	10	Assumed
$I_{FC_{max}}$	A/cm^2	600	[67]
$I_{FC_{min}}$	A/cm^2	75	[67]
$k_{1_{deg}}$	µVcm^2/A	0.243	[37,55–58]
$k_{2_{deg}}$	µV	0.159	[37,55–58]
k_{1_F}	kWcm^2/A	0.354	[57,58,67]
k_{2_F}	kW	3.837	[57,58,67]
k_{1_P}	kWcm^2/A	0.159	[57,58,67]
k_{2_P}	kWcm^2/A	7.251	[57,58,67]
$k_{11,Ah}$	1/(KAh^2)	$-7.1{\cdot}10^{-9}$	[61–63]
$k_{21,Ah}$	1/(KAh)	$2.2{\cdot}10^{-4}$	[61–63]
$k_{31,Ah}$	1/K	0.033	[61–63]
$k_{12,Ah}$	1/(KAh^2)	$2.1{\cdot}10^{-6}$	[61–63]
$k_{22,Ah}$	1/(KAh)	−0.48	[61–63]
$k_{32,Ah}$	1/K	−8.885	[61–63]
SOC_{min}	%	20	[63]
SOC_{max}	%	90	[63]
V_{batt}	m^3/kWh	0.0091	[5]
V_{FC}	m^3/kW	0.0312	[64]
V_{H_2}	m^3/kg$_{H2}$	0.025	[64,65]
V_{max}	m^3	15.5	Assumed
V_o	V	0.19	Assumed
w_{batt}	kg/kWh	8	[5]
w_{FC}	kg/kW	20	[64]
w_{H_2}	kg/kg$_{H2}$	2.5	[64,65]
w_{max}	kg	7185	Assumed

4. Results

In this section, the main results of the optimization are presented and discussed. In the first part, a comparison of the plant lifetime obtained with the proposed optimization approach and the one obtained without considering energy units degradation (i.e., non-health-conscious optimization) is presented. Afterwards, the optimal operation profile during one day of operation along the entire lifetime operation is presented and

compared with the one obtained through the non-health-conscious optimization. Lastly, the increase/decrease path of different optimization variables during the plant lifetime is analyzed.

4.1. Plant Lifetime Estimation

In this subsection, an evaluation of the energy system lifetime obtained with the proposed long-term optimization approach is compared with a non-health-conscious optimization approach. The latter considers the minimization of fuel consumption only (i.e., the minimization of the objective function f_1 in Equation (34)), and will be later referred to as FM (Fuel consumption Minimization). Figure 3 shows the SOH of both LFP batteries and PEMFC during the plant lifetime, expressed in the number of operative days. The dots indicate the SOH evaluated at the month *i*. Figure 3a shows the results of the FM optimization, while Figure 3b illustrates the results obtained with the proposed health-conscious multi-objective optimization.

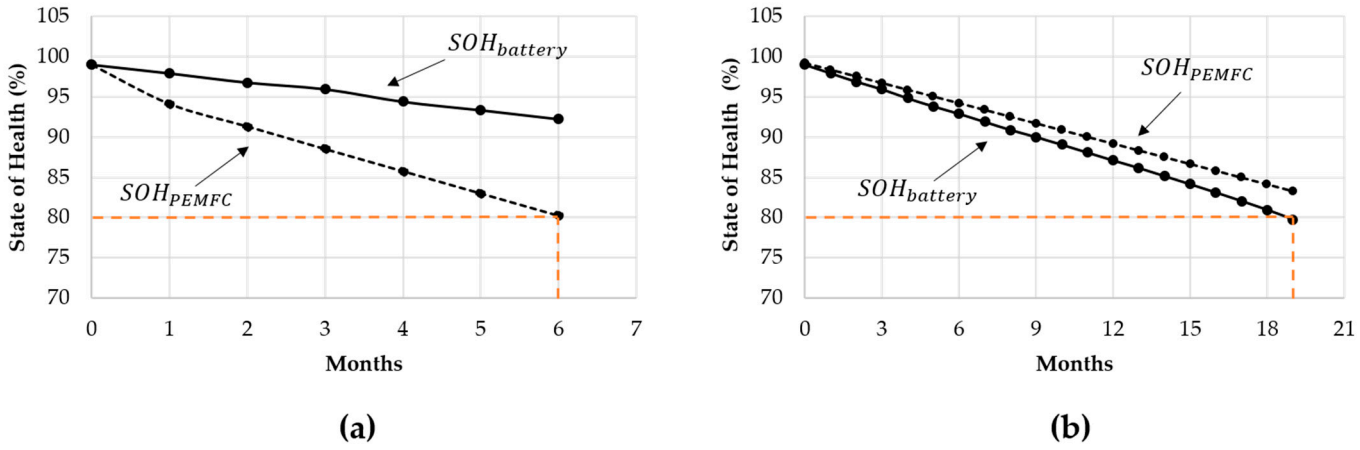

Figure 3. SOH of LFP battery and PEMFC during the plant lifetime for (**a**) fuel consumption minimization only optimization and (**b**) newly proposed long-term operation optimization approach. The dashed orange lines indicate the threshold values of SOH. The solid black lines represent the SOH of LFP battery, the dashed black lines the SOH of PEMFC.

From Figure 3a it can be noticed that with an FM approach the plant lifetime results to be about 210 days. After this time, SOH_{PEMFC} reaches 80%, while $SOH_{battery}$ is still about 93%. This is due to the fact that the design of the system is fixed following the methodology explained in [39], where battery degradation was anyway included as a constraint in the methodology. Therefore, if PEMFC degradation is not minimized the battery results to be oversized. This implies low C-rates and hence lower degradation rates of LIB. On the other hand, PEMFC stacks tend to follow the power demand. Such an operation implies that PEMFC operates at a high current density and performs large load variations, causing high degradation rates of PEMFC and hence limited lifetime.

The optimization approach proposed here allows to increase the plant lifetime from 210 to 600 operation days, as shown in Figure 3b. In this case, the first energy unit to reach the threshold value of SOH is the LFP battery, while the SOH_{PEMFC}, at this time is still about 83% (so theoretically PEMFC could work for another 60–90 days). This aspect is also due to the current higher cost of PEMFC with respect to battery (see Table 3). As a consequence, the degradation of PEMFC (f_2) weighs more on the overall objective function (f_{MO}), and hence the optimal EMS advantages the minimization of PEMFC degradation instead of the LFP battery one.

4.2. Health-Conscious Optimal Daily Operation over the Entire Lifetime

The proposed optimization approach allows also to determine the optimal daily operation of the ferry, representative for the entire month i, during the whole lifetime of the energy system.

Figure 4 shows the health-conscious optimal operation of the ferry during one day in the first month of operation (Figure 4a) and the last month of operation (Figure 4b). Here, at both the beginning and the end of the plant lifetime, the PEMFC tends to avoid the operation at rated power, as this would result in a higher degradation rate and a lower energy conversion efficiency, and tends also to avoid large load variations and start-up phases, which would also cause higher degradation rates. As for battery, it is possible to see that the operation changes from the beginning till the end of the plant lifetime. As mentioned before, the cost of battery is lower than that of PEMFC, hence the minimization of battery f_3 (Equation (36)) weighs less on the overall objective function than the minimization of PEMFC degradation f_2 (Equation (35)). As a consequence, at the beginning of the plant lifetime when the degradation rate of the battery is low, f_3 slightly affects f_{MO} (Equation (37)), and battery operates to fulfill the power demand of the ferry not covered by PEMFC. Differently, at the last month of operation, the degradation rate of the battery is higher and hence f_3 weighs more on f_{MO}. Consequently, the optimal EMS finds a compromise between the battery degradation and that of the PEMFC. For example, at the beginning of the day in the last month (Figure 4b) the PEMFC stacks operated at a higher load with respect to the first month to avoid high C-rates of the battery. To better understand the advantages of the proposed health-conscious EMS, the results of the long-term operation optimization have been compared with the results of FM optimization. Figure 5 shows the optimal operation of the ferry during one day in the first month of operation (Figure 5a) and the last month of operation (Figure 5b) if the FM approach is followed. It can be noticed that at the first month of operation (Figure 5a) the PEMFC operated to follow the highest possible value of the total energy conversion efficiency. Indeed, storing energy in the LIB would imply a lower overall efficiency, as LIB is subject to a charging/discharging efficiency. In the first month, LIB operates in a range of SOC (about 35% to 65%) smaller than in the health-conscious optimization (about 20% to 65%), and hence the LIB degradation rate is only partially affected by the non-health-conscious EMS at the beginning of the plant lifetime. In the last month of operation (Figure 5b), the situation was different. The non-health-conscious EMS would still advantage the PEMFC operation instead of LIB in order not to decrease the efficiency. However, at the end of the plant lifetime there is an increased use of LIB to overcome the voltage loss experienced by PEMFC stacks.

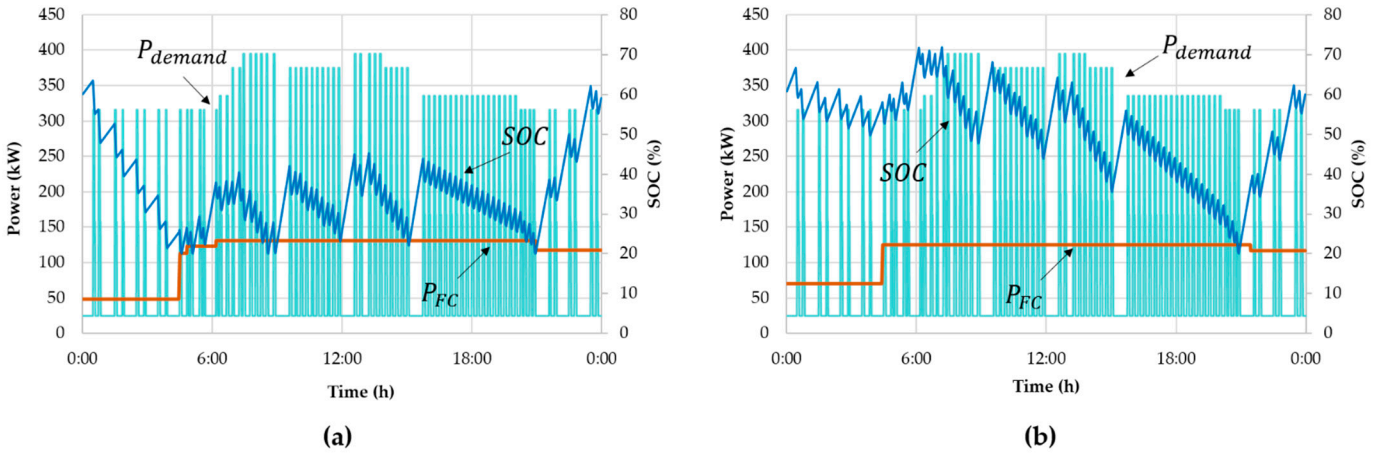

Figure 4. Health-conscious optimal daily operation of the ferry during the (**a**) first month and (**b**) last month of operation. Light blue lines represent the ferry power demand, orange lines the PEMFC output power, the blue lines the SOC of LFP battery.

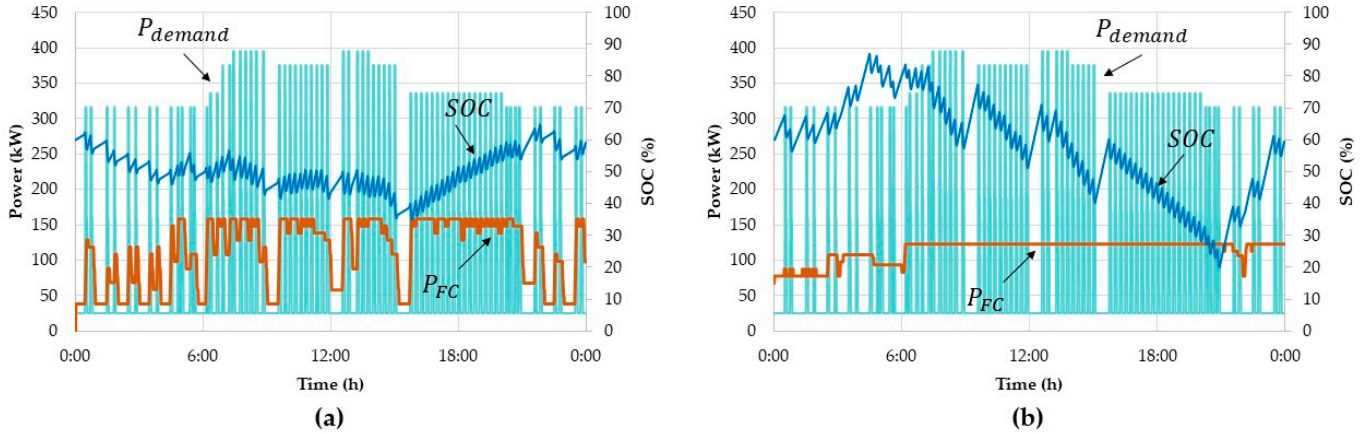

Figure 5. Non-health conscious daily optimal operation of the ferry during the (**a**) first month and (**b**) last month of operation. Light blue lines represent the ferry power demand, orange lines represent the PEMFC output power, the blue lines the SOC of LFP battery.

When focusing attention on H_2 consumption, the results show that H_2 daily consumptions obtained with the FM approach (155 kg_{H2}/day at the first month and 208 kg_{H2}/day at the last month) are similar to the ones obtained with the health-conscious approach (157 kg_{H2}/day at the first month and 204 kg_{H2}/day at the last month). This indeed demonstrates that energy conversion efficiency has not been affected considerably by limiting the degradation of PEMFC.

4.3. Behaviour of the Energy System Variables during the Plant Lifetime

As seen in Section 4.2, the proposed methodology allows to optimally define the daily operation of the ferry during the entire lifetime, and hence it is possible to analyze the behavior of the energy system variables in the long-term operation. Figure 6 shows the daily H_2 consumption (Figure 6a), the PEMFC average efficiency (Figure 6b), the volume and weight of the plant (Figure 6c), and the daily cost (Figure 6d) over time. The PEMFC average efficiency is defined as the average conversion efficiency of PEMFC over an operation day. It can be noticed that the hydrogen consumption at the end of the plant lifetime (204 kg/day) is about 29% higher than the hydrogen consumption at the beginning of the plant lifetime (157 kg/day). While this increase could be partially caused by the change in the optimal operation over time (see Section 4.2), the rise of hydrogen daily consumption is mainly due to the decrease of PEMFC average efficiency (Figure 6b). Indeed, with the progressive degradation of PEMFC, the efficiency is decreased and hence a higher amount of hydrogen is needed to reach the same power output.

An important drawback of the increase of hydrogen daily consumption over time is the increase of volume and weight required by the storage system onboard. Figure 6c reports the increase of volume and the weight of the main components of the system (i.e., LFP battery, PEMFC stacks, hydrogen tank). It is possible to observe that the system volume and weight at the end of the plant lifetime increased by up to 8.9% and 1.7%, respectively, with respect to the volume and weight at the beginning of the plant lifetime. While this does not exceed volume and weight constraints of the plant currently installed on board (Equations (5) and (6)), such aspects should be carefully taken into account when designing hybrid PEMFC propulsion systems, as it could affect the space available for the total payload of the vessel.

Lastly, from Figure 6d it is possible to see that the daily cost of the plant, i.e., the value of the f_{MO} (in Equation (37)), increases from 3183 €/day to 5518 €/day. While this increase is partially due to the increase in hydrogen daily consumption (Figure 6a), it can be mainly related to the ongoing PEMFC and LFP battery degradation over time. The average daily cost over the entire plant lifetime was calculated as being equal to 4273 €/day.

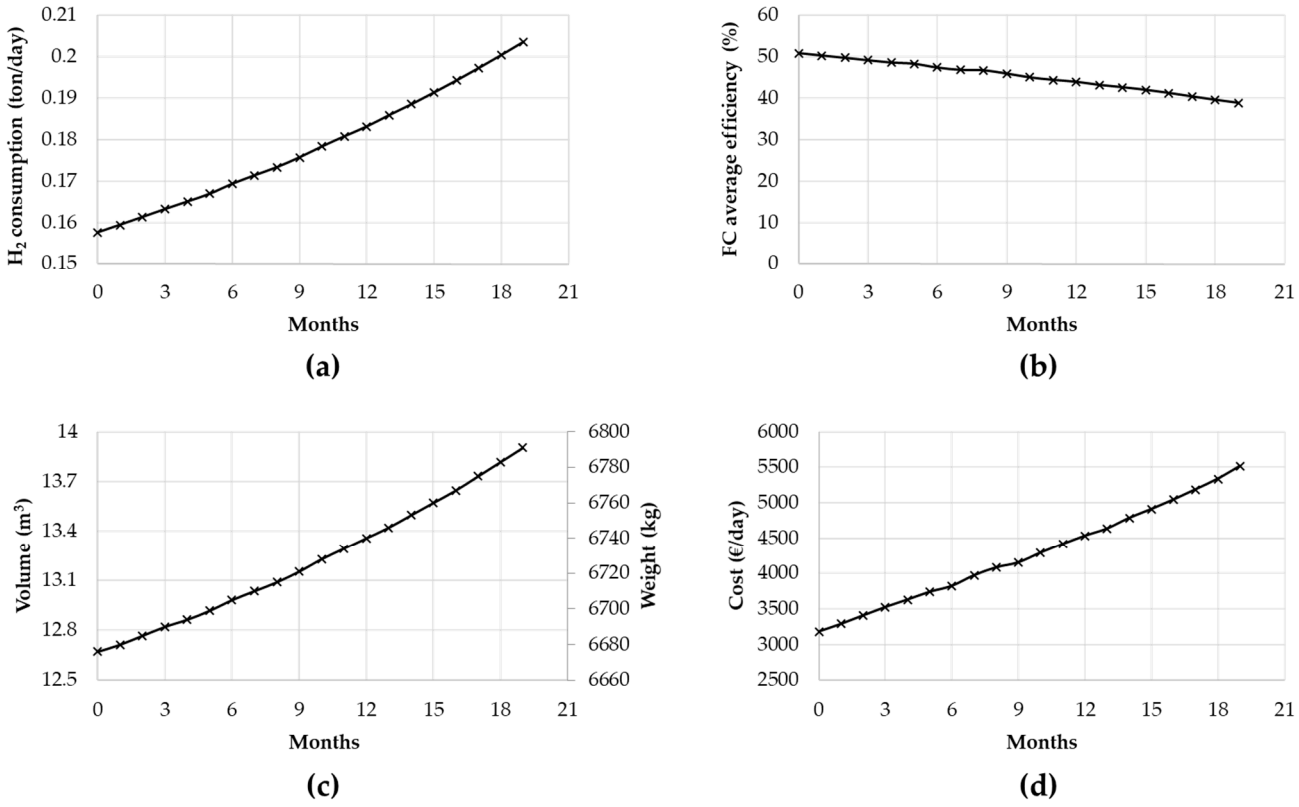

Figure 6. Energy system variables during the whole lifetime: (**a**) hydrogen daily consumption; (**b**) PEMFC average efficiency during one day; (**c**) volume and weight of the main components of the energy system; (**d**) total cost during one day of operation (value of f_{MO} in Equation (37)).

5. Conclusions

The present study proposes a new methodology for the definition of the optimal EMS over the long-term operation of hybrid PEMFC/LFP battery propulsion by developing and applying a holistic MILP optimization methodology to a small-size ferry for coastal navigation.

The proposed EMS allows to increase the overall lifetime of the plant from 210 to 600 typical operation days with respect to a FM optimization. Given the current higher cost of PEMFC in comparison with LFP battery, the first component to reach the end of life is the LFP battery system, as its degradation rate weighs less in the overall objective function of the optimization problem. The results also show that the usage of LIB helps in reducing the degradation rate of PEMFC, and plant operation changes with the passing of time to allow the optimal economic performance of the plant. With the progressive ageing of the components, the decrease in the average PEMFC efficiency causes an increase in hydrogen daily consumption (from 157 kg/day to 204 kg/day at the end of the plant lifetime). This reflects on the need to oversize the hydrogen storage system in order to ensure the daily autonomy of the ferry over the entire lifespan. Such an implication is thus jeopardizing the technical feasibility of directly installing on board the system, as well as on the cost and possible total loss of payload. Moreover, the components ageing also affects the plant daily cost, which was found to increases by up to 73% at the end of lifetime with respect to the daily cost at the beginning of the plant lifetime.

The proposed methodology is a useful tool, which can be easily adapted to other types and designs of hybrid PEMFC/LFP battery propulsion systems, as well as to other types of vessels and to other market scenarios. Moreover, the present study points out that changes in the costs of PEMFC, LFP battery and liquid hydrogen could noticeably affect the optimal long-term operation of the energy system. These results can provide some interesting inputs for future research on this topic, such as the analysis of how the

optimization results are affected by uncertainties on hydrogen, PEMC and LIB costs. In addition, the uncertainty on the mission profile, caused by variations on hull resistance (due to, e.g., fouling of ship's hull) or seasonal variability of power will also be considered in future works.

Future studies will be also addressed to the improvement of hybrid PEMFC/LIB powertrains with the addition of onboard solar energy plants and to the possible connection to a battery charging station when ferries are staying at the quay for a long time. Lastly, it should be stressed that safety and regulatory aspects still play a key role in limiting the onboard installation of such systems and hence further analyses should address these points to provide information about the technical feasibility of the plant.

Author Contributions: Conceptualization, C.D., D.P. and R.T.; methodology, C.D., D.P. and R.T.; software, C.D. and D.P.; validation, C.D., D.P. and R.T.; formal analysis, C.D., D.P. and R.T.; investigation, C.D., D.P. and R.T.; data curation, C.D. and D.P.; writing—original draft preparation, C.D., D.P. and R.T.; writing—review and editing, C.D., D.P. and R.T.; visualization, C.D., D.P. and R.T.; supervision, R.T.; project administration, R.T. All authors have read and agreed to the published version of the manuscript.

Funding: This research received no external funding.

Institutional Review Board Statement: Not applicable.

Informed Consent Statement: Not applicable.

Conflicts of Interest: The authors declare no conflict of interest.

Nomenclature

BESS	Battery Energy Storage System
DOD	Depth of Discharge
EMS	Energy Management Strategy
FM	Fuel consumption Minimization
H_2	Hydrogen
LFP	Lithium Iron Phosphate
LIB	Lithium-Ion Batteries
MILP	Mixed-Integer Linear Programming
MIQP	Mixed-Integer Quadratic Programming
NMC	Nickel Manganese Cobalt
PEMFC	Polymer Electrolyte Membrane Fuel Cells
RO-Pax	Roll-On/roll-off Passengers
SEI	Solid Electrolyte Interface
SOC	State of Charge
SOFC	Solid Oxide Fuel Cells
SOH	State of Health
Z	Generic objective function of a MILP optimization problem
$\mathbf{x}^*$	Generic continuous variable of a MILP optimization problem
$\boldsymbol{\delta}^*$	Generic binary variable of a MILP optimization problem
$\mathbf{g}$	Equality constraints of a generic MILP optimization problem
$\mathbf{h}$	Inequality constraints of a generic MILP optimization problem
t	Time
P_{demand}	Propulsion and auxiliary power demand of the ferry
j	Index for PEMFC stacks
P_{FC}	Power output of a PEMFC stack
P_{batt}^{+}	Discharging power of LIB
P_{batt}^{-}	Charging power of LIB
n	Number of PEMFC stacks
t_{in}	Initial time step for one day of operation
t_{fin}	Last time step of one day of operation

F_{FC}	Fuel consumption of a PEMFC stack
$P_{FC_{max}}$	PEMFC stack rated power
V_{H_2}	Volume occupied by the hydrogen storage
V_{FC}	Volume occupied by a PEMFC stack
V_{batt}	Volume occupied by LIB
w_{H_2}	Weight of bunkered hydrogen
w_{FC}	Weight of a PEMFC stack
w_{batt}	Weight of LIB
c_{ov}	Oversizing correction factor
I_{FC}	Current density of PEMFC stack
k_{1F}, k_{2F}	Linearization coefficients
$k_{1P}, \ k_{2P}$	Linearization coefficients
δ_{FC}	Binary variable defining on/off status of PEMFC stacks
$\delta_{st.\ up}$	Binary variable defining the occurrence of PEMFC start-up phase
F_{start}	Fuel consumption in a start-up phase
$I_{FC_{min}}$	Lower limit of PEMFC current density
$I_{FC_{max}}$	Upper limit of PEMFC current density
$\Delta_{P_{FC}}$	Allowed load variation of a PEMFC stack
dV_{load}	PEMFC voltage loss due to load variation
Δv_{load}	Proportionality constant
$\Delta v_{st,up}$	Proportionality constant
$dV_{st,up}$	PEMFC voltage loss due to start-up
$dV_{P_{FC}}$	PEMFC voltage loss due to power load
$k_{1_{dv}}, k_{2_{dv}}$	Linearization coefficients
dV	Total loss of voltage of PEMFC (not cumulative)
dV_{TOT}	Cumulative loss of voltage of PEMFC
$k_{1_{deg}}, k_{2_{deg}}$	Linearization coefficients
$V_{ref,FC}$	Reference maximum voltage for new PEMFC
η_{FC}	PEMFC stack efficiency
E_{batt}	Energy stored in LIB
η_{batt}	Charging/discharging efficiency of LIB
$E_{battery_{max}}$	Energy capacity of LIB
Δt	Time interval between two consecutive time steps
$Crate^{\pm}$	C-rate of LIB in charging/discharging phase
$Crate_{max}$	Upper limit on LIB C-rate
SOC_{cal}	SOC constraint to limit the calendar ageing
T_{batt}	Temperature of LIB
$a_{1T,x}, \ a_{2T,x}$	Linearization coefficients
Q_{loss}	Capacity fade of LIB
T_{amb}	Ambient temperature
a_{1QT}, a_{2QT}	Linearization coefficients
Ah	Energy throughput of LIB
$k_{11,Ah}, \ k_{21,Ah}, k_{31,Ah}$	Proportionality constants
$k_{12,Ah}, \ k_{22,Ah}, k_{32,Ah}$	Proportionality constants
n_{days}	Number of days per month
N_{cycle}	Number of equivalent cycles of LIB
Ah_{cell}	Capacity of a LIB single cell
SOC_{min}	Lower limit on SOC
SOC_{max}	Upper limit on SOC
w_1, w_2, w_3	Weights of the objective functions
f_1, f_2, f_3	Objective functions
f_{MO}	Blended objective function
c_{H_2}	Cost of hydrogen
c_{batt}	Cost of LIB
c_{FC}	Cost of PEMFC
V_o	PEMFC loss of voltage allowed before substituting PEMFC
$Q_{loss_{max}}$	Maximum capacity fade before substituting LIB

Appendix A

In the following, details on the ferry chosen as a case study are reported for convenience, while extensive information is available in [39]. Figure A1 shows the power demand profile of the ferry for a typical day of operation. The considered ferry has been assumed to operate 72 journeys per day, each with a duration of five minutes. The propulsion power demand while sailing has been evaluated as a function of typical sailing speeds obtained by fitting the speed data available in [68]. It has been assumed that the sailing phase can be divided into two phases: a first phase at high power and a second one in which the power demand is reduced thanks to the draft. It has been assumed that only auxiliary power is required while the ship is in port. Auxiliary power has been set to 25 kW, constant during the day. In order to account for possible variations in the sea conditions during the day, it has been assumed that the power demand is higher in the central hours of the day due to increased sea-traffic in the area.

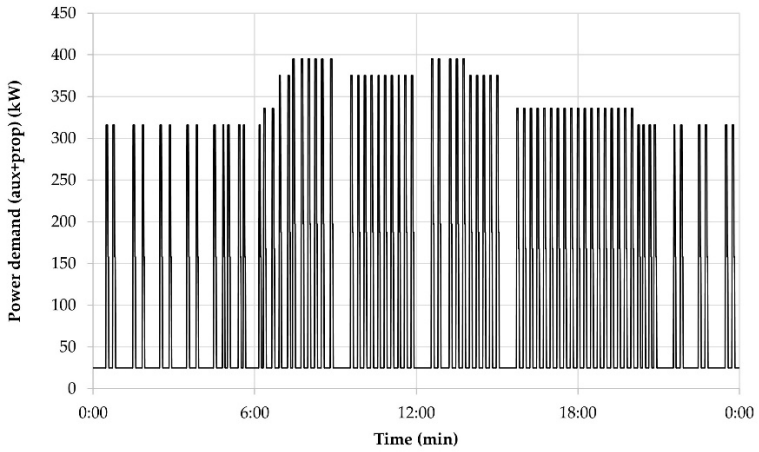

Figure A1. Power demand profile of the ferry chosen as a case study [39].

References

1. Van Biert, L.; Godjevac, M.; Visser, K.; Aravind, P.V. A review of fuel cell systems for maritime applications. *J. Power Source* **2016**, *327*, 345–364. [CrossRef]
2. Tronstad, T.; Åstrand, H.H.; Haugom, G.P.; Langfeldt, L. *Study on the Use of Fuel Cells in Shipping*; European Maritime Safety Agency: Lisboa, Portugal, 2017.
3. Dall'Armi, C.; Micheli, D.; Taccani, R. Comparison of different plant layouts and fuel storage solutions for fuel cells utilization on a small ferry. *Int. J. Hydrogen Energy* **2021**, *46*, 13878–13897. [CrossRef]
4. Anwar, S.; Zia, M.Y.I.; Rashid, M.; de Rubens, G.Z.; Enevoldsen, P. Towards Ferry Electrification in the Maritime Sector. *Energies* **2020**, *13*, 6506. [CrossRef]
5. European Maritime Safety Agency (EMSA). *Study on Electrical Energy Storage for Ships*; EMSA: Lisboa, Portugal, 2020.
6. Elektra Project: Ballard Receives PO from BEHALA for 3 × 100 kW Fuel Cell Modules to Power German Push Boat. Available online: https://www.ballard.com/about-ballard/newsroom/news-releases/2019/10/02/ballard-receives-po-from-behala-for-3-x-100kw-fuel-cell-modules-to-power-german-push-boat (accessed on 12 January 2021).
7. Elektra Project: Brennstoffzellen an Bord von Schiffen. Available online: https://www.e4ships.de/english/inland-shipping/elektra/ (accessed on 12 January 2021).
8. Energy Observer. Available online: https://www.energy-observer.org/ (accessed on 12 January 2021).
9. Energy Observer: Energy Balance Nassau—Fort-de-France. Available online: https://www.energy-observer.org/innovations/navigation-nassau-fort-de-france (accessed on 12 January 2021).
10. Sjø, B. Rapport fase 2 Utviklingskontrakt utslippsfri hurtigbåt. In *Doffin 2017-138144 Brødrene Aa Westcon Power & Automation*; 2017; Available online: https://www.trondelagfylke.no/contentassets/bd8d4260feb14f6bb7503ddc6360e168/brodrene-aa-sluttrapport-offentlig.pdf (accessed on 19 April 2020).
11. Brødrene Aa Presents the "AERO" a Newly Developed Hydrogen Fast Ferry Concept—Fuel Cells Works. Available online: https://fuelcellsworks.com/news/brodrene-aa-presents-the-aero-a-newly-developed-hydrogen-fast-ferry-concept/ (accessed on 12 January 2021).
12. Race for Water—A Foundation to Preserve Water. Available online: https://www.raceforwater.org/en/ (accessed on 12 January 2021).

13. Future Proof Shipping—Creating a Zero-Emissions Shipping World. Available online: https://www.futureproofshipping.com/ (accessed on 12 January 2021).
14. Toyota Tsusho Conducts Joint Research with Yanmar on Fuel Cell System for Boats—Toward the Creation of a Hydrogen Society by Expanding the Use of Hydrogen. Available online: https://www.toyota-tsusho.com/english/press/detail/180326_004178.html (accessed on 12 January 2021).
15. Ballard Fuel Cell Modules Used in Successful Yanmar Boat Test to Support Development of Safety Guidelines in Japan. Available online: https://www.prnewswire.com/news-releases/ballard-fuel-cell-modules-used-in-successful-yanmar-boat-test-to-support-development-of-safety-guidelines-in-japan-678507543.html (accessed on 12 January 2021).
16. Water-Go-Round. Available online: https://watergoround.com/ (accessed on 12 January 2021).
17. SW/TCH Maritime. Available online: https://www.switchmaritime.com/ (accessed on 16 March 2021).
18. Enova Banebrytende Samarbeid Gir Millioner til Utslippsfri Teknologi. Available online: https://www.enova.no/pilot-e/banebrytende-samarbeid-gir-millioner-til-utslippsfri-maritim-teknologi/ (accessed on 12 January 2021).
19. Enova PILOT-E. Available online: https://www.enova.no/pilot-e/ (accessed on 12 January 2021).
20. Madsen, R.T.; Klebanoff, L.E.; Caughlan, S.A.M.; Pratt, J.W.; Leach, T.S.; Appelgate, T.B.; Kelety, S.Z.; Wintervoll, H.C.; Haugom, G.P.; Teo, A.T.Y.; et al. Feasibility of the Zero-V: A zero-emissions hydrogen fuel-cell coastal research vessel. *Int. J. Hydrogen Energy* **2020**, *45*, 25328–25343. [CrossRef]
21. Sandia Energy Maritime Applications for Hydrogen Fuel Cells. Available online: https://energy.sandia.gov/programs/sustainable-transportation/hydrogen/fuel-cells/maritime-applications/ (accessed on 12 January 2021).
22. Choi, C.H.; Yu, S.; Han, I.S.; Kho, B.K.; Kang, D.G.; Lee, H.Y.; Seo, M.S.; Kong, J.W.; Kim, G.; Ahn, J.W.; et al. Development and demonstration of PEM fuel-cell-battery hybrid system for propulsion of tourist boat. *Int. J. Hydrogen Energy* **2016**, *41*, 3591–3599. [CrossRef]
23. Zemship Project Website. Available online: https://ec.europa.eu/environment/life/project/Projects/index.cfm?fuseaction=search.dspPage&n_proj_id=3081 (accessed on 24 April 2020).
24. Vogler, F.; Würsig, G. Fuel cells in maritime applications: Challenges, chances and experiences. In Proceedings of the 4th International 527 Conference on Hydrogen Safety (ICHS), San Francisco, CA, USA, 12–14 September 2011.
25. Zemship Project. One Hundred Passengers and Zero Emissions—The First ever Passenger Vessel to Sail Propelled by Fuel Cells, 2013. Available online: https://webgate.ec.europa.eu/life/publicWebsite/index.cfm?fuseaction=search.dspPage&n_proj_id=3081 (accessed on 19 April 2020).
26. Fuel Cell Boat, Amsterdam, The Netherlands. Available online: http://www.opr-advies.nl/fuelcellboat/efcbboot.html (accessed on 12 January 2021).
27. He, Y.; Miao, C.; Wu, J.; Zheng, X.; Liu, X.; Liu, X.; Han, F. Research on the Power Distribution Method for Hybrid Power System in the Fuel Cell Vehicle. *Energies* **2021**, *14*, 734. [CrossRef]
28. Sorlei, I.S.; Bizon, N.; Thounthong, P.; Varlam, M.; Carcadea, E.; Culcer, M.; Iliescu, M.; Raceanu, M. Fuel Cell Electric Vehicles—A Brief Review of Current Topologies and Energy Management Strategies. *Energies* **2021**, *14*, 252. [CrossRef]
29. Taccani, R.; Malabotti, S.; Dall'Armi, C.; Micheli, D. High energy density storage of gaseous marine fuels: An innovative concept and its application to a hydrogen powered ferry. *Int. Shipbuild. Prog.* **2020**, *67*, 29–52. [CrossRef]
30. Han, J.; Charpentier, J.-F.; Tang, T. An Energy Management System of a Fuel Cell/Battery Hybrid Boat. *Energies* **2014**, *7*, 2799–2820. [CrossRef]
31. Bassam, A.M.; Phillips, A.B.; Turnock, S.R.; Wilson, P.A. An improved energy management strategy for a hybrid fuel cell/battery passenger vessel. *Int. J. Hydrogen Energy* **2016**, *41*, 22453–22464. [CrossRef]
32. Rivarolo, M.; Rattazzi, D.; Lamberti, T.; Magistri, L. Clean energy production by PEM fuel cells on tourist ships: A time-dependent analysis. *Int. J. Hydrogen Energy* **2020**, *45*, 25747–25757. [CrossRef]
33. Rivarolo, M.; Rattazzi, D.; Magistri, L. Best operative strategy for energy management of a cruise ship employing different distributed generation technologies. *Int. J. Hydrogen Energy* **2018**, *43*, 23500–23510. [CrossRef]
34. Bassam, A.M.; Phillips, A.B.; Turnock, S.R.; Wilson, P.A. Development of a multi-scheme energy management strategy for a hybrid fuel cell driven passenger ship. *Int. J. Hydrogen Energy* **2017**, *42*, 623–635. [CrossRef]
35. Zhang, Z.; Guan, C.; Liu, Z. Real-Time Optimization Energy Management Strategy for Fuel Cell Hybrid Ships Considering Power Sources Degradation. *IEEE Access* **2020**, *8*, 87046–87059. [CrossRef]
36. Chen, H.; Zhang, Z.; Guan, C.; Gao, H. Optimization of sizing and frequency control in battery/supercapacitor hybrid energy storage system for fuel cell ship. *Energy* **2020**, *197*. [CrossRef]
37. Wu, P.; Bucknall, R. Hybrid fuel cell and battery propulsion system modelling and multi-objective optimisation for a coastal ferry. *Int. J. Hydrogen Energy* **2020**, *45*, 3193–3208. [CrossRef]
38. Wu, P.; Partridge, J.; Bucknall, R. Cost-effective reinforcement learning energy management for plug-in hybrid fuel cell and battery ships. *Appl. Energy* **2020**, *275*, 115258. [CrossRef]
39. Pivetta, D.; Dall'Armi, C.; Taccani, R. Multi-objective optimization of hybrid PEMFC/Li-ion battery propulsion systems for small and medium size ferries. *Int. J. Hydrogen Energy* **2021**. In Press. [CrossRef]
40. Kandidayeni, M.; Macias, A.; Boulon, L.; Trovão, J.P.F. Online modeling of a fuel cell system for an energy management strategy design. *Energies* **2020**, *13*, 3713. [CrossRef]

41. Ghobadpour, A.; Amamou, A.; Kelouwani, S.; Zioui, N.; Zeghmi, L. Impact of powertrain components size and degradation level on the energy management of a hybrid industrial self-guided vehicle. *Energies* **2020**, *13*, 5041. [CrossRef]
42. Fletcher, T.; Ebrahimi, K. The Effect of Fuel Cell and Battery Size on Efficiency and Cell Lifetime for an L7e Fuel Cell Hybrid Vehicle. *Energies* **2020**, *13*, 5889. [CrossRef]
43. Çınar, H.; Kandemir, I. Active energy management based on meta-heuristic algorithms of fuel cell/battery/supercapacitor energy storage system for aircraft. *Aerospace* **2021**, *8*, 85. [CrossRef]
44. Liang, J.; Li, Y.; Jia, W.; Lin, W.; Ma, T. Comparison of Two Energy Management Strategies Considering Power System Durability for PEMFC-LIB Hybrid Logistics Vehicle. *Energies* **2021**, *14*, 3262. [CrossRef]
45. Wang, Y.; Moura, S.J.; Advani, S.G.; Prasad, A.K. Power management system for a fuel cell/battery hybrid vehicle incorporating fuel cell and battery degradation. *Int. J. Hydrogen Energy* **2019**, *44*, 8479–8492. [CrossRef]
46. Li, H.; Ravey, A.; N'Diaye, A.; Djerdir, A. Online adaptive equivalent consumption minimization strategy for fuel cell hybrid electric vehicle considering power sources degradation. *Energy Convers. Manag.* **2019**, *192*, 133–149. [CrossRef]
47. Yue, M.; Jemei, S.; Gouriveau, R. Review on health-conscious energy management strategies for fuel cell hybrid electric vehicles: Degradation models and strategies. *Int. J. Hydrogen Energy* **2019**, *44*, 6844–6861. [CrossRef]
48. Ito, K.; Yokoyama, R.; Shiba, T. Optimal operation of a diesel engine cogeneration plant including a heat storage tank. *J. Eng. Gas Turbines Power* **1992**, *114*, 687–694. [CrossRef]
49. Rech, S. Smart Energy Systems: Guidelines for Modelling and Optimizing a Fleet of Units of Different Configurations. *Energies* **2019**, *12*, 1320. [CrossRef]
50. Pivetta, D.; Rech, S.; Lazzaretto, A. Choice of the Optimal Design and Operation of Multi-Energy Conversion Systems in a Prosecco Wine Cellar. *Energies* **2020**, *13*, 6252. [CrossRef]
51. Rech, S.; Lazzaretto, A. Smart rules and thermal, electric and hydro storages for the optimum operation of a renewable energy system. *Energy* **2018**, *147*, 742–756. [CrossRef]
52. Python. Available online: https://www.python.org/ (accessed on 24 March 2021).
53. Gurobi Optimization. Available online: https://www.gurobi.com/ (accessed on 16 March 2021).
54. Jouin, M.; Bressel, M.; Morando, S.; Gouriveau, R.; Hissel, D.; Péra, M.; Zerhouni, N.; Jemei, S.; Hilairet, M.; Ould, B. Estimating the end-of-life of PEM fuel cells: Guidelines and metrics. *Appl. Energy* **2016**, *177*, 87–97. [CrossRef]
55. Lorenzo, C.; Bouquain, D.; Hibon, S.; Hissel, D. Synthesis of degradation mechanisms and of their impacts on degradation rates on proton-exchange membrane fuel cells and lithium-ion nickel—Manganese—Cobalt batteries in hybrid transport applications. *Reliab. Eng. Syst. Saf.* **2021**, *212*, 107369. [CrossRef]
56. Balestra, L.; Schjølberg, I. Modelling and simulation of a zero-emission hybrid power plant for a domestic ferry. *Int. J. Hydrogen Energy* **2021**, *46*, 10924–10938. [CrossRef]
57. Fletcher, T.; Thring, R.; Watkinson, M. An Energy Management Strategy to concurrently optimise fuel consumption & PEM fuel cell lifetime in a hybrid vehicle. *Int. J. Hydrogen Energy* **2016**, *41*, 21503–21515. [CrossRef]
58. Chen, H.; Pei, P.; Song, M. Lifetime prediction and the economic lifetime of proton exchange membrane fuel cells. *Appl. Energy* **2015**, *142*, 154–163. [CrossRef]
59. Al-gabalawy, M.; Mahmoud, K.; Darwish, M.M.F.; Dawson, J.A.; Lehtonen, M.; Hosny, N.S. Reliable and robust observer for simultaneously estimating state-of-charge and state-of-health of lifepo4 batteries. *Appl. Sci.* **2021**, *11*, 3609. [CrossRef]
60. Redondo-Iglesias, E.; Venet, P.; Pelissier, S. Calendar and cycling ageing combination of batteries in electric vehicles. *Microelectron. Reliab.* **2018**, *88–90*, 1212–1215. [CrossRef]
61. Wang, J.; Liu, P.; HIcks-Garner, J.; Sherman, E.; Soukiazan, S.; Verbrugge, M.; Tataria, H.; Musser, J.; Finamore, P. Cycle-life model for graphite-LiFePO4 cells. *J. Power Source* **2011**, *196*, 3942–3948. [CrossRef]
62. Dubarry, M.; Qin, N.; Brooker, P. Calendar aging of commercial Li-ion cells of different chemistries—A review. *Curr. Opin. Electrochem.* **2018**, *9*, 106–113. [CrossRef]
63. Groot, J. *State-of-Health Estimation of Li-Ion Batteries: Ageing Models*; Chalmers University of Technology: Gothenburg, Sweden, 2014.
64. Internation Energy Agency (IEA). *The Future of Hydrogen*; IEA: Paris, France, 2019.
65. International Renewable Energy Agency (IRENA). *Green Hydrogen Cost Reduction*; IRENA: Abu Dhabi, United Arab Emirates, 2020.
66. Ioannis, T.; Dalius, T.; Natalia, L. *Li-Ion Batteries for Mobility and Stationary Storage Applications—Scenarios for Costs and Market Growth*; Publications Office of the European Union: Luxembourg, 2018; ISBN 9789279972546.
67. Wang, G.; Huang, F.; Yu, Y.; Wen, S.; Tu, Z. Degradation behavior of a proton exchange membrane fuel cell stack under dynamic cycles between idling and rated condition. *Int. J. Hydrogen Energy* **2018**, *43*, 4471–4481. [CrossRef]
68. Marine Traffic. Available online: https://www.marinetraffic.com/ (accessed on 19 April 2020).